# A3G-2021-186431
# 11 May 2021
# Rudder Tube Kt

DISTRIBUTION STATEMENT A. Approved for public release: distribution unlimited.
Public Release Memo: 2021-09-10_WAA-0011

Prepared By:

X STOWE.GREGORY.L.1152688390 Digitally signed by STOWE.GREGORY.L.1152688390 Date: 2021.10.25 10:36:44 -06'00'

Connor N. Hood
AFLCMC/WAAECC A-10 Analysis Group

Review By:

X STOWE.GREGORY.L.1152688390 Digitally signed by STOWE.GREGORY.L.1152688390 Date: 2021.10.25 10:36:57 -06'00'

Greg Stowe
AFLCMC/WAAECC A-10 Analysis Group

X THOMSEN.MARK.L.1255235091 Digitally signed by THOMSEN.MARK.L.1255235091 Date: 2021.10.25 12:07:43 -06'00'

Mark Thomsen
AFLCMC/WAAEC A-10 A-10 Analysis Group

**TABLE OF CONTENTS**

# List of Figures

## 1.0 Introduction

The stress concentration due to a corrosion pit within a tube subject to a bending moment was determined for multiple corrosion pit geometries using finite element models (FEMs). Figure 1 provides a schematic of the loading condition and corrosion pit location. The corrosion pit was located on the tension side of the bending moment. Table 1 specifies the corrosion pit geometries that were investigated.

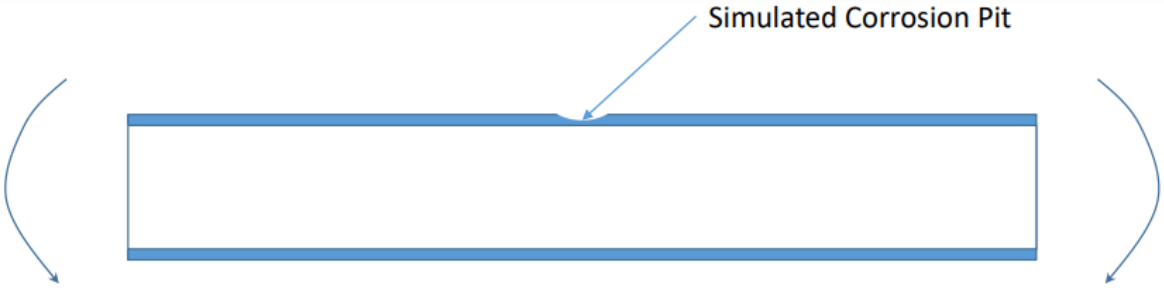


**Figure 1: Loading Condition & Corrosion Pit Location**

**Table 1: Pit Geometries Investigated**

| Pit Diameter (in.) | Pit Depth (in.) |
|---|---|
| 0.018 | 0.0035 |
| 0.018 | 0.007 |
| 0.018 | 0.014 |
| 0.018 | 0.028 |
| 0.018 | 0.035 |
| 0.035 | 0.0035 |
| 0.035 | 0.007 |
| 0.035 | 0.014 |
| 0.035 | 0.028 |
| 0.035 | 0.035 |

## 2.0 Geometry & Mesh

### 2.1 Solid Models

Each model was identical with the exception of the corrosion pit dimensions. The geometry for each model is defined within Figure 2 and Figure 3. Additionally, the model dimensions are outlined within Table 2.

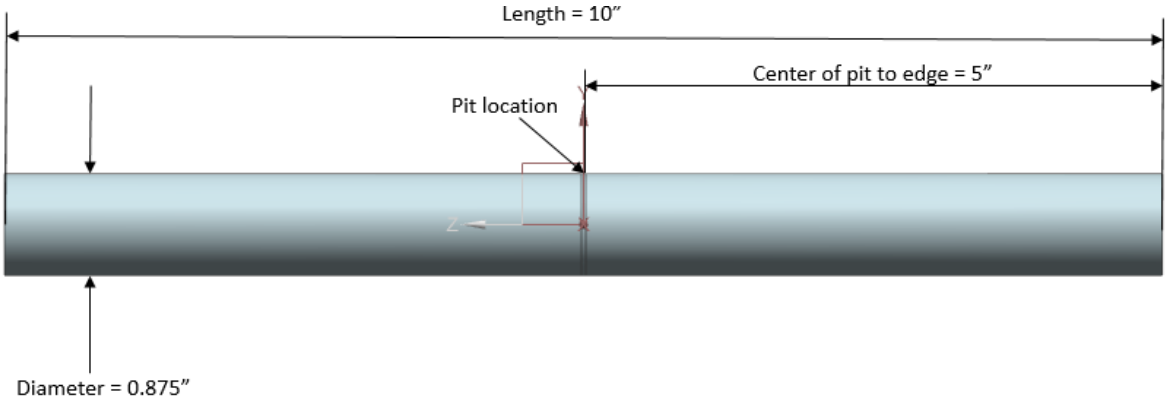


**Figure 2: Model Geometry Definitions 1**

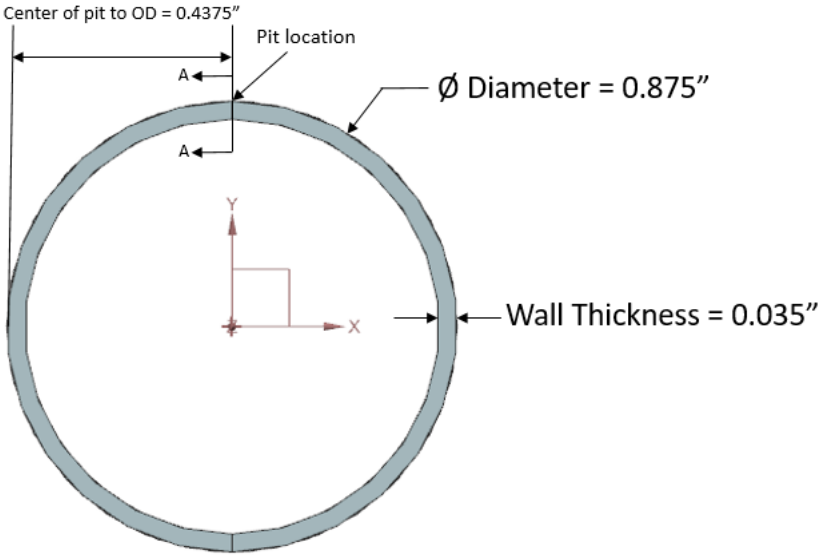


**Figure 3: Model Geometry Definitions 2**

**Table 2: Model Dimensions**

| | |
|---|---|
| Length | 10" |
| Diameter | 0.875" |
| Wall Thickness | 0.035" |
| Center of pit to edge | 5" |
| Center of pit to OD | 0.4375" |

The corrosion pit location for each model is specified within Figure 2 and Figure 3. The dimensions for the corrosion pit are defined within Figure 4, section A-A is specified within Figure 3. The body was split using the three planes specified within Figure 5, Figure 6, and Figure 7 in order to investigate stresses and refine the mesh near the corrosion pit.

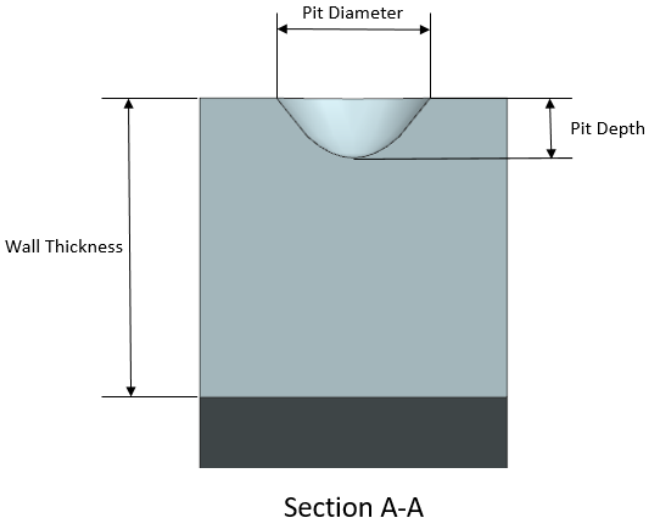


**Figure 4: Corrosion Pit Geometry**

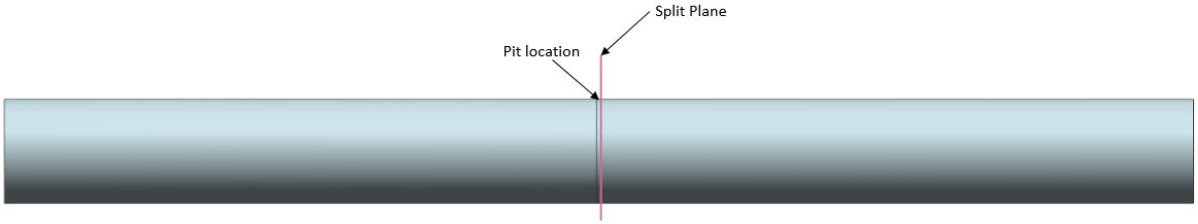


**Figure 5: Split Body 1**

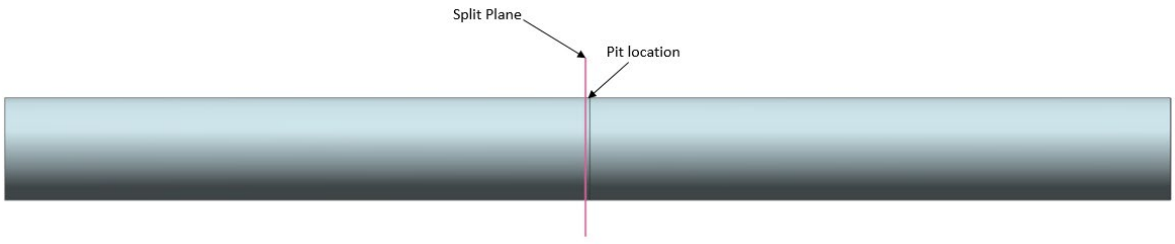


**Figure 6: Split Body 2**

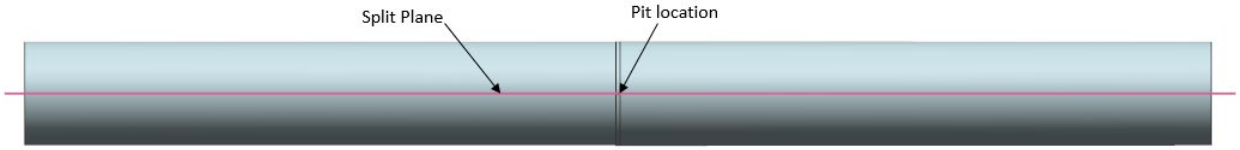


**Figure 7: Split Body 3**

### 2.2 Finite Element Models

The three bodies specified within Figure 8 were meshed using CTETRA(10) elements. The mesh size for each body is specified within Table 3. Additionally, there were two mesh controls applied to the model which are outlined within Table 4. The first mesh control was a face density of .005" applied to the two faces specified within Figure 9. The second mesh control was a face density of .010" applied to the four faces specified within Figure 10. Lastly, there was an RBE2 element added at one end of the tube, seen within Figure 11. The resulting mesh is provided within Figure 12 and Figure 13.

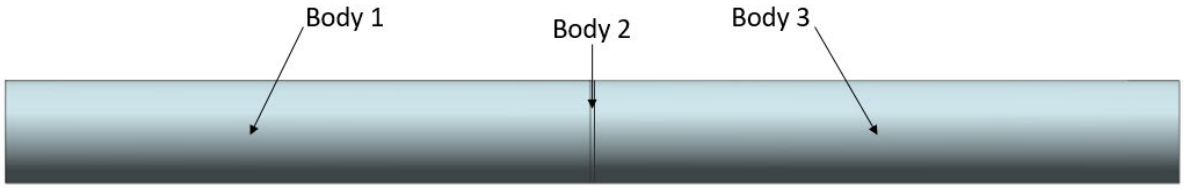


**Figure 8: Meshed Bodies**

**Table 3: Seed Mesh Sizes**

| Body | Mesh Size (in.) |
|---|---|
| 1 | 0.093 |
| 2 | 0.01 |
| 3 | 0.093 |

**Table 4: Mesh Controls**

| Mesh Control | Location |
|---|---|
| Face Density = .005" | Specified within Figure 9 |
| Face Density = .010" | Specified within Figure 10 |

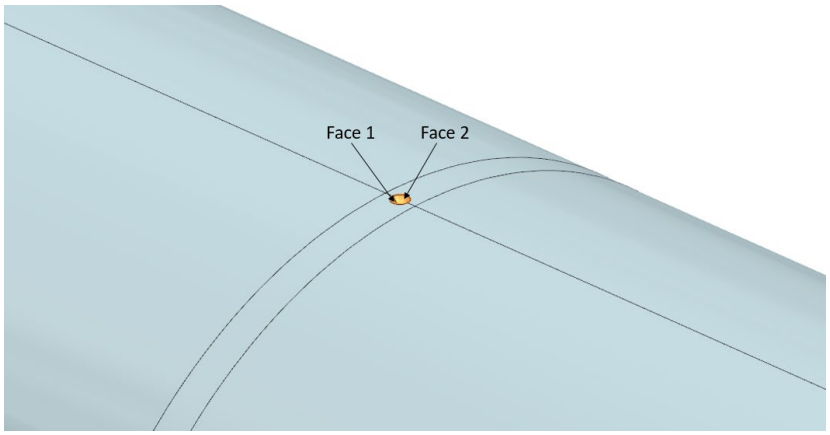


**Figure 9: Mesh Control 1 Locations**

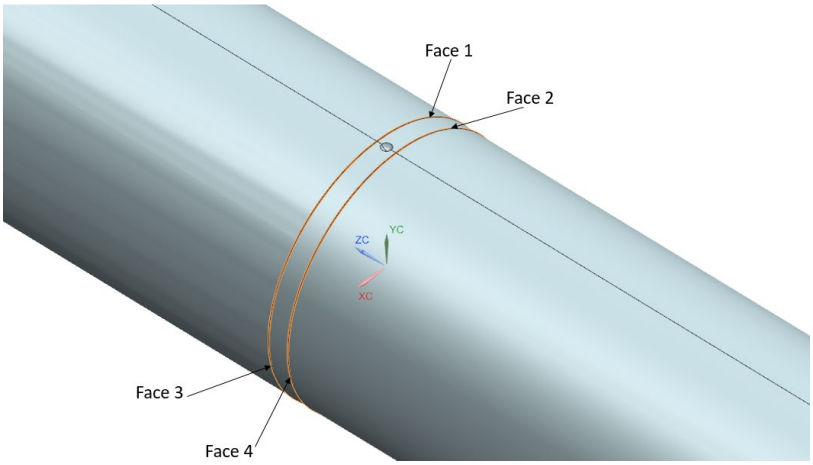


**Figure 10: Mesh Control 2 Locations**

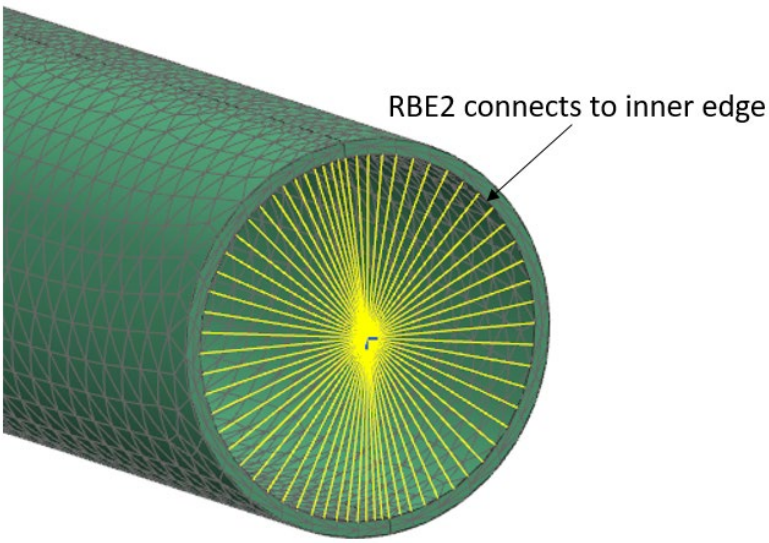


**Figure 11: RBE2 Connection**

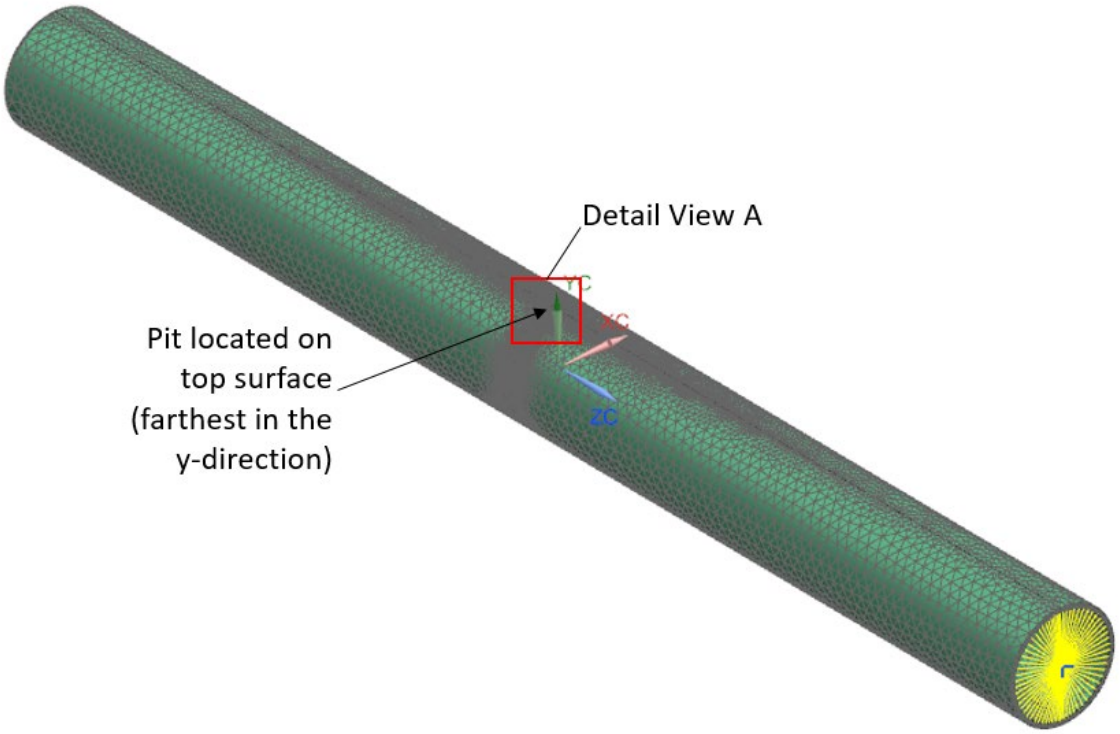


**Figure 12: Finalized Mesh**

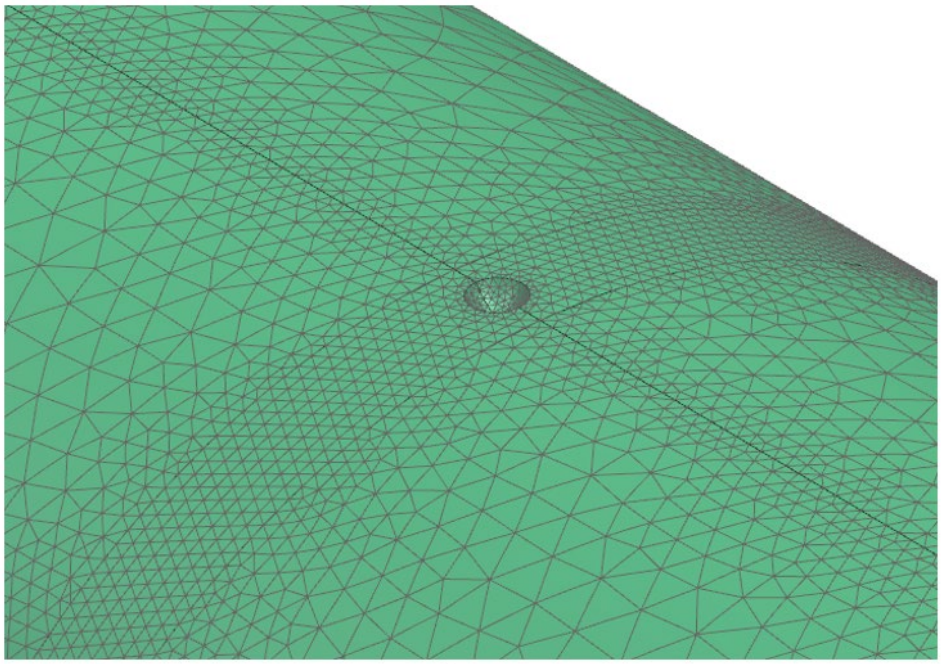

Detail View A

**Figure 13: Finalized Mesh – Detail View A**

## 3.0 Boundary Conditions & Loads

### 3.1 Boundary Conditions

There was one boundary condition applied throughout the entire model. The face specified within Figure 14 had a fixed boundary condition.

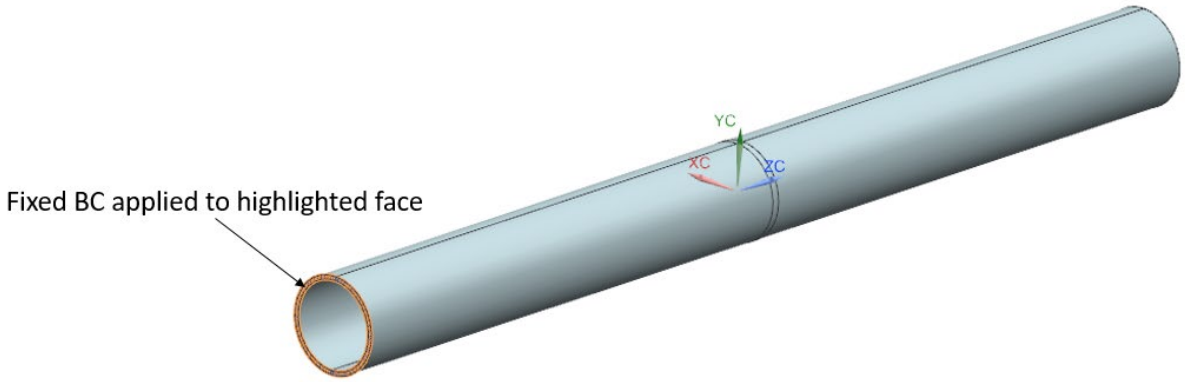


**Figure 14: Boundary Condition Application Location**

### 3.2 Loads

There was one load applied throughout the entire model. The node specified within Figure 15 had a positive 1,000 in-lbs moment applied about the x-axis.

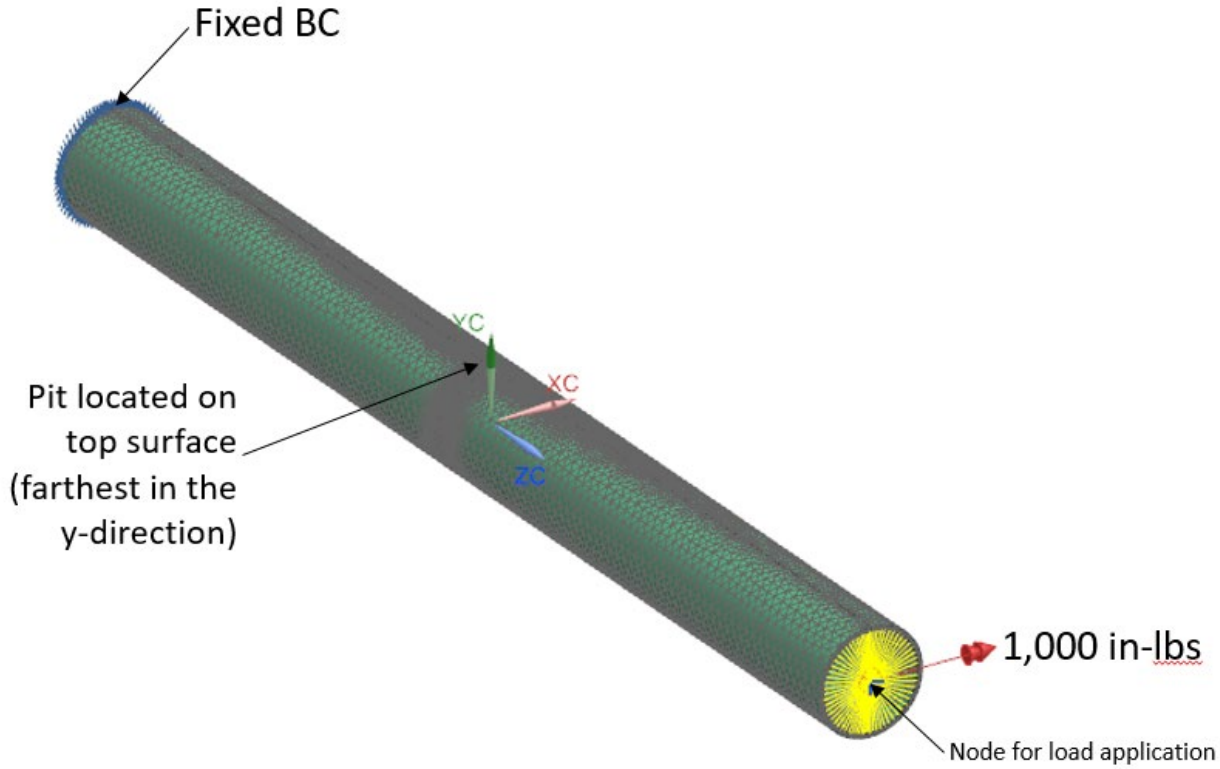


**Figure 15: Load Application Location**

## 4.0 Mesh Convergence

Mesh convergence was checked for the smallest pit geometry. It was assumed that if mesh convergence occurs on the smallest pit geometry, then it occurs for all pit geometries. This was a reasonable assumption because the mesh size and mesh controls for each pit geometry were the same. Mesh convergence was checked by calculating the percent difference, using Equation 1.

**Equation 1: Percent Difference**

$$Percent\ Difference = \frac{stress\ convergence\ model - stress\ nominal\ model}{stress\ convergence\ model} * 100$$

Where,

$$stress\ convergence\ model = \max stress\ near\ pit\ location\ within\ convergence\ model$$

$$stress\ nominal\ model = \max stress\ near\ pit\ location\ within\ nominal\ model$$

The nominal model used the seed mesh and face density mesh sizes specified within Table 3 and Table 4, respectively. The convergence model used the seed mesh sizes specified within Table 3 and used the face density mesh sizes specified within Table 4 divided by 2. The nominal model and convergence model meshes are shown within Figure 16 and Figure 17, respectively.

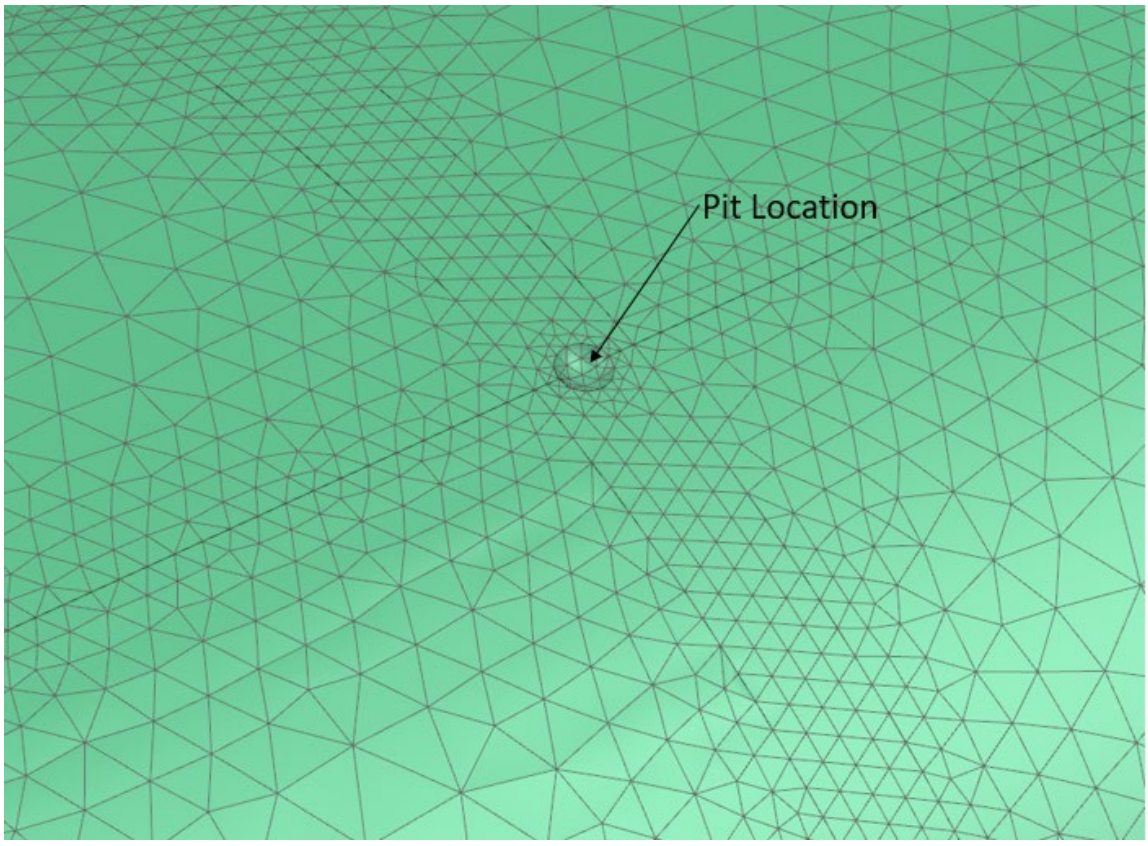


**Figure 16: Nominal Mesh near Pit Location**

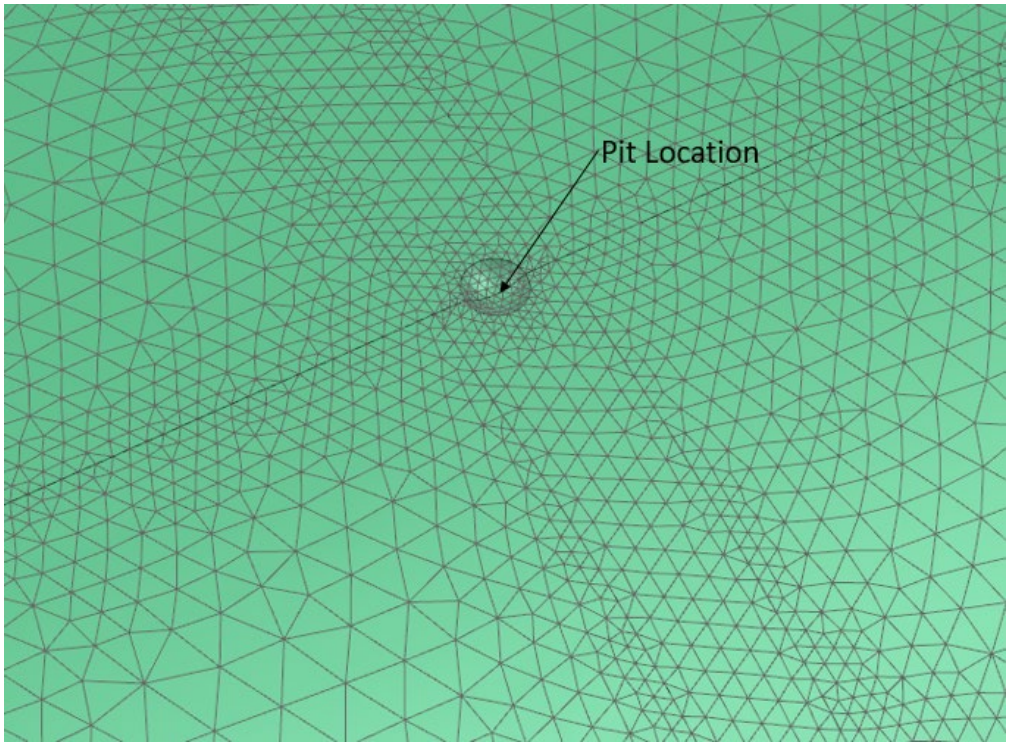


**Figure 17: Convergence Mesh near Pit Location**

The contour plot and maximum stress for the nominal and convergence models are provided within Figure 18 and Figure 19, respectively. The percent difference was calculated to be 4.47%, therefore, the nominal mesh was considered converged.

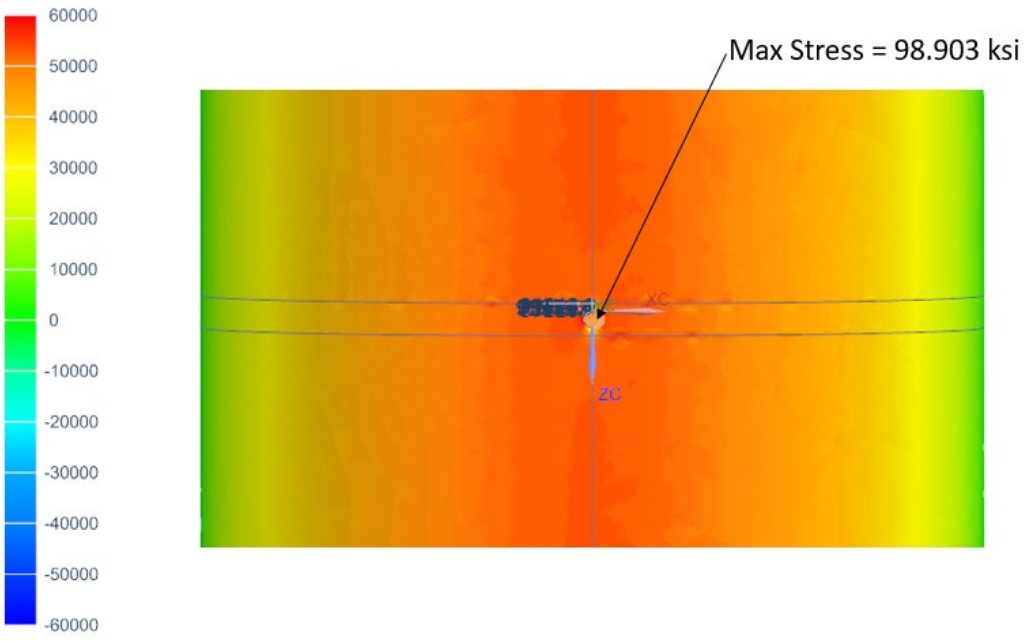


**Figure 18: Nominal Model Contour Plot**

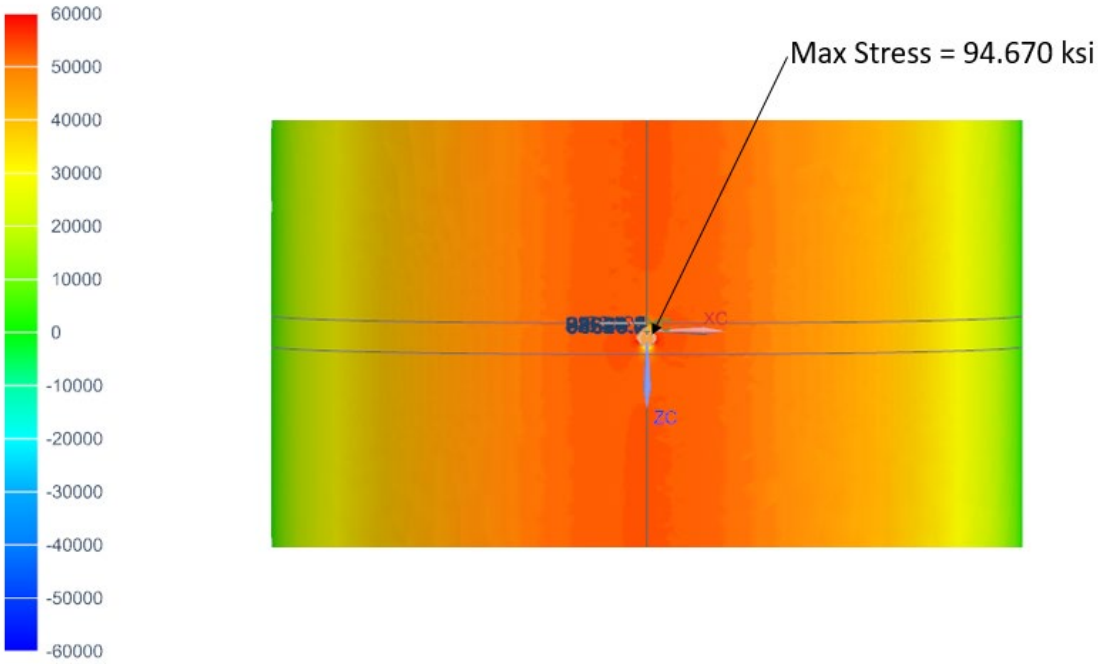


**Figure 19: Convergence Model Contour Plot**

## 5.0 Loads Verification

The stresses at the pit location were compared between the nominal model and the closed form solution to verify that the loads were applied correctly to the FEM. The nominal model stress was determined from the selection specified within Figure 20, each element selected is on the outer surface. The closed form solution stress was calculated using Equation 2. The percent difference between the nominal model stress and closed form solution stress is .08% providing confidence that the loads were applied correctly.

**Equation 2: Bending Stress at Pit Location**

$$\sigma_{pit} = \frac{M_{applied} C_{pit}}{I_{tube}}$$

Where,

$$\sigma_{pit} = bending\ stress\ at\ pit\ location$$

$$M_{applied} = applied\ beding\ moment = 1{,}000\ in - lbs$$

$$I_{tube} = moment\ of\ inertia\ of\ tube$$

Thus,

$$\sigma_{pit} = \frac{(1{,}000)(0.4375)}{\frac{\pi}{64}(.875^4 - .805^4)} = 53{,}612\ psi$$

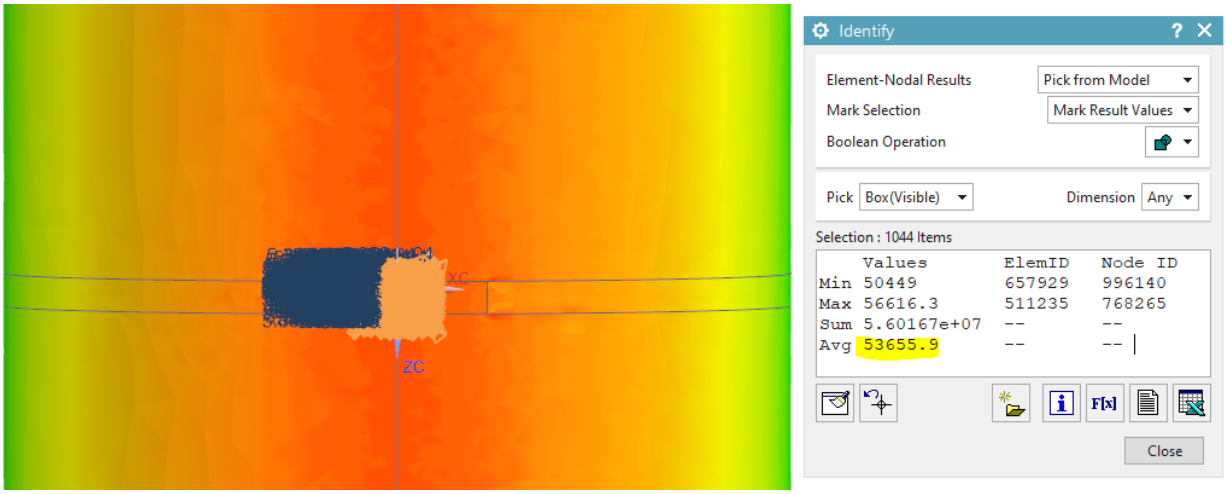


**Figure 20: Nominal Model Stress Extraction**

## 6.0 Stress Concentrations

The stress concentration for each pit geometry was calculated using Equation 3. The max stress was extracted using Stress – Element – Nodal – Max Principal and selecting the elements within the black box specified within Figure 21. The selection was made using Identify Results – Pick – Box (All), specified within Figure 22. The stress concentrations for pit diameters of .018" and .035" are provided within Table 5 and Table 6, respectively. Figure 23 plots stress concentration vs. pit depth for each pit diameter.

**Equation 3: Stress Concentration**

$$Stress\ Concentration = \frac{Max\ Pit\ Stress}{Max\ Nominal\ Stress}$$

Where,

$$Max\ Pit\ Stress = \max stress\ in\ pit\ model$$
$$Max\ Nominal\ Stress = \max stress\ in\ nominal\ model$$

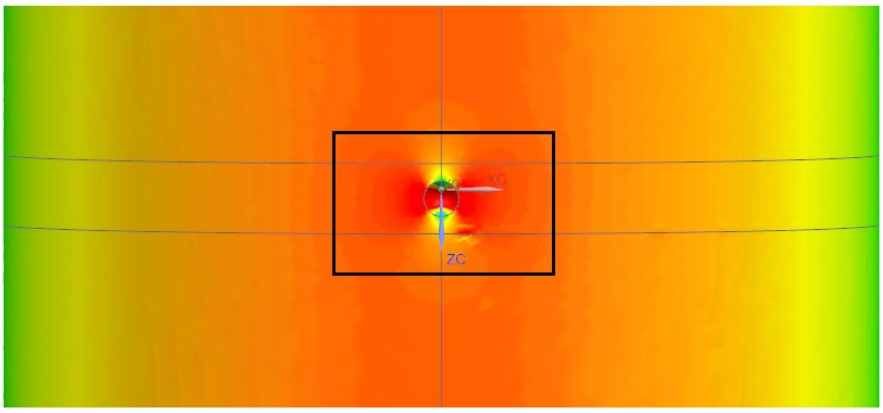

**Figure 21: Selection Area to Determine Max Stress**

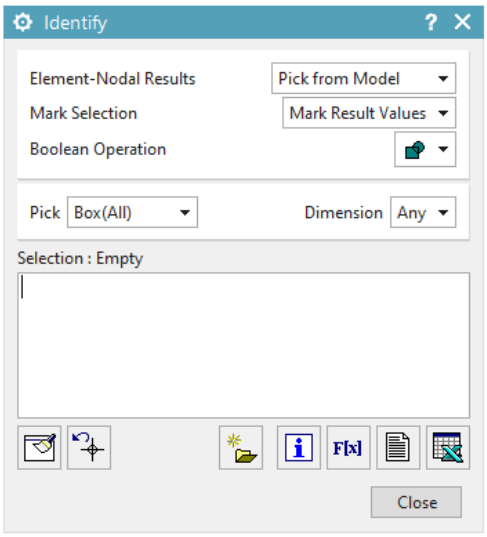


**Figure 22: Selection Settings to Determine Max Stress**

**Table 5: Stress Concentrations – Pit Diameter .018”**

| Pit Diameter = 0.018" | | | |
|---|---|---|---|
| Pit Depth (in.) | Nominal Stress (ksi) | Max Stress (ksi) | Kt |
| 0 | 56.616 | 56.616 | 1 |
| 0.0035 | 56.616 | 93.428 | 1.650 |
| 0.007 | 56.616 | 121.002 | 2.137 |
| 0.014 | 56.616 | 145.767 | 2.575 |
| 0.028 | 56.616 | 161.768 | 2.857 |
| 0.035 | 56.616 | 174.744 | 3.087 |

**Table 6: Stress Concentrations – Pit Diameter .035”**

| Pit Diameter = 0.035" | | | |
|---|---|---|---|
| Pit Depth (in.) | Nominal Stress (ksi) | Max Stress (ksi) | Kt |
| 0 | 56.616 | 56.616 | 1 |
| 0.0035 | 56.616 | 76.097 | 1.344 |
| 0.007 | 56.616 | 105.944 | 1.871 |
| 0.014 | 56.616 | 122.184 | 2.158 |
| 0.028 | 56.616 | 148.591 | 2.625 |
| 0.035 | 56.616 | 169.414 | 2.992 |

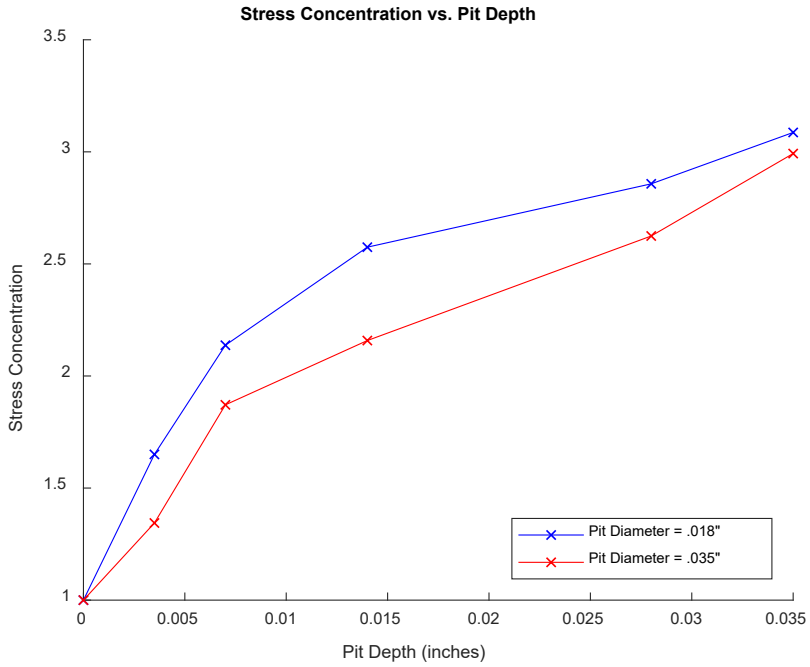


**Figure 23: Stress Concentration vs. Pit Depth**

## 7.0 Conclusion

The stress concentration was determined for multiple corrosion pit geometries within a tube when it is subject to a bending moment. The stress concentration for each corrosion pit diameter converged to 3 as the pit depth approached the wall thickness. The stress concentration for both pit diameters was ~3 once the pit perforated agreeing with Peterson's stress concentration for a hole in an infinite plate.